JOURNAL OF Applied Polymer SCIENCE

Thermal and Dielectric Studies of PEG/C/AST Nanocomposites

Panagiotis Klonos,[1] Stelios Kaprinis,[1] Vladimir I. Zarko,[2] Vassilis Peoglos,[1] Evgenij M. Pakhlov,[2] Polycarpos Pissis,[1] Vladimir M. Gun'ko[2]

[1]Department of Physics, National Technical University of Athens, 15780 Athens, Greece

[2]Department of Amorphous and Structurally Ordered Oxides, Chuiko Institute of Surface Chemistry, Kiev 03164, Ukraine

Correspondence to: V. M. Gun'ko (E-mail: vlad_gunko@ukr.net)

ABSTRACT: C/AST/PEG nanocomposites with fumed AST (89 wt % Al_2O_3, 10 wt % SiO_2, 1 wt % TiO_2), activated carbon, and poly(-ethylene glycol), PEG, were prepared in a wide range of PEG and C/AST (1 : 9) contents. Thermal transitions (mainly in a PEG phase) were investigated by differential scanning calorimetry. The dynamic behavior was investigated by thermally stimulated depolarization current and dielectric relaxation spectroscopy. The PEG crystallinity degree decreases in the nanocomposites, in particular at $C_{PEG} \leq 40$ wt %. A significant fraction of amorphous polymer is immobilized at a filler surface making no contribution to the glass transition, whereas the rest exhibits a lower glass transition temperature, when compared with bulk polymer, because of loosened molecular packing of the chains. Several relaxations arising from the polymer matrix, the filler, and their combination were identified and analyzed. The segmental α-relaxation of the PEG matrix was found to become faster in the nanocomposites. © 2012 Wiley Periodicals, Inc. J. Appl. Polym. Sci. 000: 000–000, 2012

KEYWORDS: calorimetry; composites; interfaces; relaxation; activation energy

Received 18 January 2012; accepted 23 April 2012; published online
DOI: 10.1002/app.37956

INTRODUCTION

Nanooxides, such as fumed individual silica, titania, alumina and related mixed oxides, are used in industry, medicine, biotechnology, and cosmetics as individual materials or components in composites with polymers and/or low-molecular organics.[1–9] Polymer/nanooxide composites can be prepared using aqueous or organic suspensions, nanopowders impregnated by a polymer solution, polymerization of monomers or oligomers, or polymer cross-linking in the presence of nanooxides. Activated carbons (ACs) are used as individual adsorbents or in composition with polymers, e.g., AC covered by a polymer semipermeable membrane to improve AC biocompatibility.[10,11] Solid (oxide or AC) nanoparticle–nanoparticle interactions in upper hierarchical structures (aggregates, agglomerates, microparticles, and granules) depend on a variety of factors including surface structure, the degree of chemical binding of particle–particle or particle–polymer, the amounts of water or other solvents, temperature and pressure of treatments, and presence and characteristics of polymers. Many of these characteristics, especially related to the interfacial behavior of polymers and low-molecular compounds, can be studied by differential scanning calorimetry (DSC), thermally stimulated depolarization current (TSDC), and dielectric relaxation spectroscopy (DRS).

In different applications, polymers can be used as solid surface modifiers at a low content or the main materials in core (solid)–shell (polymer) particles or monolith. Poly(ethylene glycol), PEG, or a similar polymer as poly(ethylene oxide), PEO, as water-soluble polar heteropolymers are used alone or in composites with other polymers, oxides, carbons, or other fillers in many industrial, medical, and other applications. PEG–PEG or PEO–PEO interactions are much weaker than their hydrogen or van der Waals bonding to solid particles because these polymers do not have hydroxyls.[12] Therefore, PEG can be well distributed (Figure 1) at a surface of solid particles because stronger interactions of PEG with oxide surfaces. However, in the case of porous materials, polymer penetration into pores, especially nanopores, is slow and restricted because of confined space effects, polymer sizes, and interaction time. Features of the system organization with polymer/filler or solid nanoparticles with immobilized polymers affect the polymer dynamics, thermodynamic and other properties of the composites.

There are several types of secondary (γ and β) and primary (α) relaxations in glass-forming materials[13,14] appearing with increasing temperature and affected by the confined space. Smaller structures (polar bonds due to their rotations[15,16]) are responsible for the γ-relaxation, and larger structures (polymer

© 2012 Wiley Periodicals, Inc.

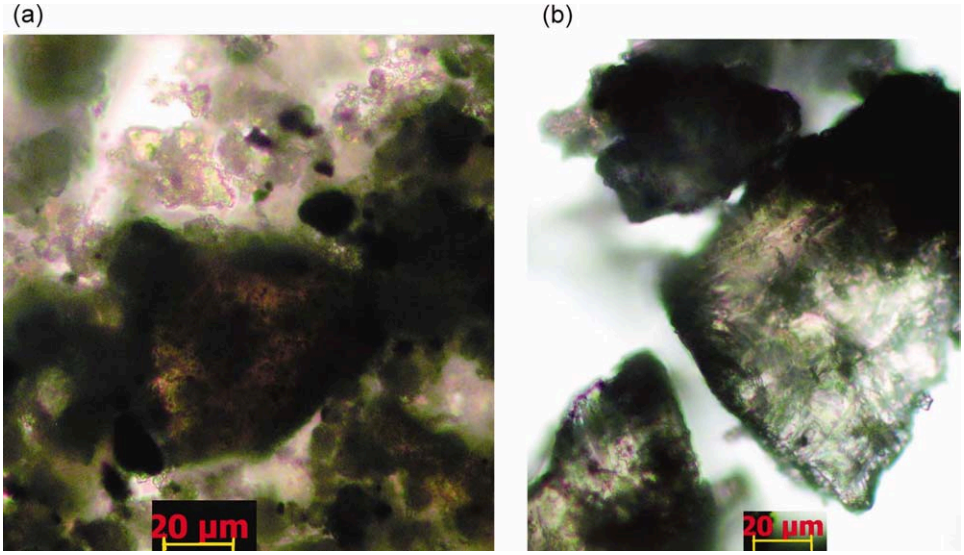

Figure 1. Microphotographs (Primo Star optical microscope, Carl Zeiss) show representative samples: (a) C/AST/PEG-4 (90/10) and (b) C/AST/PEG-4 (10/90) (bar 20 μm). [Color figure can be viewed in the online issue, which is available at wileyonlinelibrary.com.]

fragments with bound water) participate in β-relaxation. Therefore, the γ-relaxation is faster (with a time scale on the order of picoseconds at room temperature) than β-relaxation and occurs at lower temperatures in isochronal (constant frequency) experiments.[17–21] The main α-relaxation (dynamic glass transition[14]) occurring at temperatures higher than the glass transition temperature (T_g) is characterized by the nonexponential (e.g., stretched-exponential) time dependence and the non-Arrhenius temperature dependence of relaxation time expressed by, e.g., the Vogel-Tammann-Fulcher equation.[22–24] The Johari-Goldstein process (β_{JG})[25] decoupled from the α-process appears roughly below T_g, and the relaxation time shows Arrhenius temperature dependence, i.e., without the cooperative effects. An interfacial polarization or Maxwell–Wagner–Sillars (MWS) relaxation process[14] was identified for temperatures above the glass transition and the α-relaxation. The effects of confined space for polymers penetrating into pores result in changes in both temperature and frequency dependences of the relaxations. Notice that adsorbed water can strongly affect these phenomena because of plasticization of polymers and changes in polymer–oxide interactions.[15,16] This is due to penetration of water molecules between macromolecules and solid surface or between polymers that results in the formation of a more flexible hydrogen network in comparison with the dry system. A combination of DSC, TSDC, and DRS can allow us deeper insight into the interfacial behavior of polymer/oxide/AC composites studied.

Feng et al.[26] prepared shape-stabilized phase change materials composed of PEG and mesoporous AC using blending and impregnating method. These materials are characterized by decreased activation energy of the PEG phase change with increasing PEG content, and the phase change properties were influenced by the confinement of the PEG segments adsorbed in pores of AC. Composites of AC with PEO and PEG demonstrate dependence of the characteristics on the molecular weight of the polymers.[27] The PEG adsorption onto AC depends on molecular weight, temperature, and pH and can be well described with the Langmuir model.[28] PEG can be also used in graphene–sulfur–polymer composite as rechargeable lithium-sulfur battery cathode material.[29] In these materials, the PEG-graphene layers are important for accommodating volume expansion of the coated sulfur particles during discharge, trapping soluble polysulfide intermediates, and rendering the sulfur particles electrically conducting. Notice that a PEG interfacial layer can be less dense than poly(vinyl alcohol), PVA, because the latter can form strong hydrogen PVA–PVA bonds.[30–33] Previous comparative investigations of PEG-Al_2O_3/SiO_2/TiO_2 and A-300-PEG composites showed[34] that local interactions between polymer and AST are stronger than that of polymer–polymer. It is of interest to study changes in the behavior of PEG in PEG/nanooxide composites because of addition of a relatively small (with respect to nanooxide fraction) amount of AC. Despite many publications, there is no information on such composites as PEG-nanooxide-AC. Notice that nanooxide-AC composites prepared in a microbreaker were found to preserve the structural characteristics related to nanopores and mesopores in AC and textural porosity of nanooxides.[35] It is of interest what is the effect of AC (10 wt % in the mixture with nanooxide) in the AC-Al_2O_3/SiO_2/TiO_2–PEG systems because the textural characteristics of nanooxides and AC are very different that can provide unexpected results in the composites (important for practical applications). Therefore, the aim of this article was to study the interfacial behavior of PEG of different molecular weight at the surface of Al_2O_3/SiO_2/TiO_2-AC composite using thermal and dielectric techniques: DSC, TSDC, and DRS.

EXPERIMENTAL

Materials

C/AST/PEG consists of fumed AST (89 wt % Al_2O_3, 10 wt % SiO_2, and 1 wt % TiO_2, S_{BET} = 99 m^2/g),[36] activated carbon, AC (40% burn-off, S_{BET} = 1520 m^2/g) (MAST Carbon

International Ltd., UK),[37–39] and PEG (with two molecular weights 35 and 4 kDa, PEG-35 and PEG-4, respectively). Nanocomposite C/AST was prepared by mechanochemical activation (MCA) (treatment in a microbreaker during only 3 min to prevent deeper destruction of the AC microtexture). Nanocomposite C/AST includes 10 wt % of AC and 90 wt % of AST.

The aqueous suspension of C/AST was sonicated (22 kHz) for 3 min. Then, the solution of PEG (5 wt %) in amounts corresponding to 10, 20, 40, 60, 80, and 90 wt % of the polymer with respect to dry C/AST was added at room temperature. The suspensions were dried for 5–10 days depending on the amount of water. The PEG amount at $C_{PEG} = 20$ wt % is enough to form a monolayer coverage (according to FTIR, TG, and TPD mass-spectrometry data[33–37]) of oxide and AC nanoparticles. Thus, the systems can be separated into two classes, namely with $C_{PEG} \leq 40$ wt % and $C_{PEG} \geq 60$ wt %, which can be considered as PEG adsorbed on silica and AC particles and PEG filled by oxide/AC filler, respectively. Polymer macromolecules on C/AST particles [Figure 1(a)] or filler particles are distributed in the polymer matrix [Figure 1(b)] are well distributed. However, the systems are microheterogeneous. Figure 1 shows representative samples since images for other compositions are similar to that shown.

Differential Scanning Calorimetry

Glass transition and crystallization/melting of PEG in the nanocomposites were investigated in nitrogen atmosphere in the temperature range from −120 to 120°C using a TA Q200 series DSC instrument. Dried powder samples (∼ 8 mg) were closed in standard Tzero aluminium pans. Cooling and heating rates were fixed at 10°C/min in standard measurements. Aiming to suppress the degree of crystallinity of PEG, measurements were also performed with fast cooling (quenching). For these measurements, the cooling rate was not constant over the whole temperature range. However, the cooling rate in the crystallization temperature region (0–40°C), which is of interest here, was ∼ 75°C/min. Before recording, these thermal scans (1st, 2nd, and quenching) samples were heated to 80°C to erase thermal history of PEG, as the crystallization temperature of PEG is close to room temperature: (i) 1st scan: 80°C → −120°C → 120°C (1 min isothermal stay at 80°C); (ii) 2nd scan: 120°C → −120°C → 120°C (1 min isothermal stay at 120°C); and (iii) quenching: 100°C → −105°C → 100°C (1 min isothermal stay at 100°C).

The DSC thermograms were evaluated in terms of the transition temperatures and the corresponding enthalpy changes.[40] The heat capacity step at the glass transition was normalized to an amorphous polymer fraction ($\Delta c_{p,am}$),

$$\Delta c_{p,am} = \frac{\Delta c_{p,DSC}}{(1 - X_{cr}) C_{PEG}/100}, \quad (1)$$

where X_{cr} is the crystallinity degree calculated from the melting enthalpy, ΔH_{DSC}, and the enthalpy of PEG fusion, ΔH_0,[41]

$$X_{cr} = \frac{\Delta H_{DSC}}{\Delta H_0 \cdot C_{PEG}/100}. \quad (2)$$

The fraction of immobilized polymer, X_{im}, defined as a fraction of amorphous polymer, which does not contribute to the glass transition, was calculated as

$$X_{im} = \left(1 - \frac{\Delta c_{p,am}}{\Delta c_{p,am(PEG)}}\right)(1 - X_{cr}) \quad (3)$$

where $\Delta c_{p,am}$ refers to the nanocomposites, $\Delta c_{p,am(PEG)}$ is the corresponding quantity for the neat polymer sample, and $C_{PEG}/100$ is the weight fraction of the polymer in the composite. The fractions of immobilized polymer, amorphous and total, are given by equations

$$X_{im,amorph} = \left(1 - \frac{\Delta c^{ncp}_{p,norm}}{\Delta c^{PEG}_{p,norm}}\right) \quad (4)$$

$$X_{im,polymer} = \left(1 - \frac{\Delta c^{ncp}_{p,norm}}{\Delta c^{PEG}_{p,norm}}\right)(1 - X_{cr}) \quad (5)$$

where $\Delta C^{ncp}_{p,norm}$ is the heat capacity step for the nanocomposite.

Thermally Stimulated Depolarization Current

The TSDC method is a dielectric technique in the temperature domain, characterized by a high sensitivity and a high resolving power. The latter is due to its low equivalent frequency (10^{-4}–10^{-2} Hz).[42] A sample was inserted between the brass plates of a capacitor, placed in a Novocontrol TSDC sample cell and polarized by the electrostatic field at $E_p \approx 10^5$ V/m with a homemade voltage source at polarization temperature $T_p = 20$°C for time $t_p = 5$ min (standard measurements). Measurements were also carried out under different polarization temperatures. With the field still applied, the sample was cooled down to −150°C (cooling rate was 10°C/min under a nitrogen flow), sufficiently low to prevent depolarization by thermal energy, then short-circuited and reheated to 30°C at a constant heating rate $b =$ 3°C/min. Temperature control was achieved by means of a Novocontrol Quatro cryosystem. Discharge current was generated during heating and measured as a function of temperature with a sensitive programmable Keithley 617 electrometer. The TSDC measurements were performed using thin cylindrical pellets (13 mm in diameter, ∼ 1 mm in thickness and 0.8–2.0 g cm^{-3} in density) pressed using a PerkinElmer pressure cell at 10^4 atm. Before measurements, the pellets were equilibrated at ambient conditions. Measurements were also carried out on samples dried either in a vacuum oven at 80°C for 2 h or in a dessicator over P_2O_5.

Dielectric Relaxation Spectroscopy

For DRS[43] measurements, samples (similar to used in the TSDC measurements) were placed between the plates of a capacitor and alternating voltage was applied in a Novocontrol sample cell. The complex dielectric permittivity, $\varepsilon^* = \varepsilon' - i\varepsilon''$, where ε' and ε'' are the real and imaginary parts, respectively, was recorded isothermally as a function of frequency in the 10^{-1} to 10^6 Hz range at temperatures −150 to 30°C (in nitrogen atmosphere) in steps of 5 and 10°C (depending on a process studied) using a Novocontrol Alpha analyzer. The temperature was

Applied Polymer SCIENCE

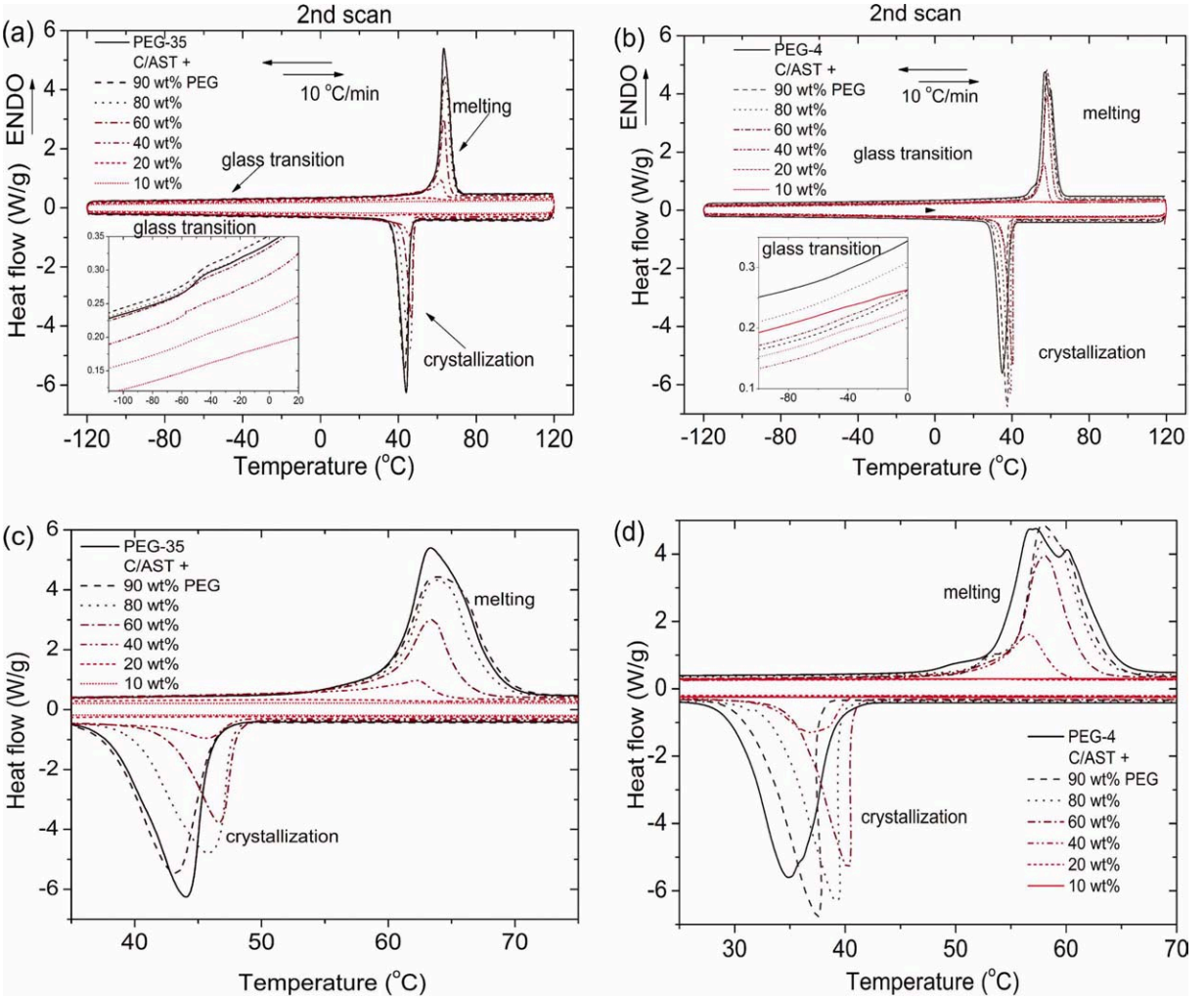

Figure 2. DSC thermograms recorded on the C/AST/PEG-35 (a) and C/AST/PEG-4 (b) nanocomposites indicated on the plots (scan 2—after linear cooling with10°C/min). The insets show details in the glass transition region. Details in the crystallization/melting region are shown in (c) and (d). [Color figure can be viewed in the online issue, which is available at wileyonlinelibrary.com.]

controlled better than ±0.5°C with a Novocontrol Quatro cryosystem.

RESULTS AND DISCUSSION

DSC Measurements

Results of DSC measurements for all the materials studied are shown as raw data (cooling and heating thermograms) in Figure 2 and results of evaluation in Figure 3. Glass transition temperatures T_g were determined as the midpoint of the heat capacity step at glass transition,[40] whereas the crystallization and melting temperatures, T_c and T_m, respectively, were determined as the peak temperatures. The glass transition temperature interval, $\Delta T_g = T_{end} - T_{onset}$, where T_{end} and T_{onset} are the temperature values which limit the glass transition event during heating, is a measure of the width of the glass transition process and provides information on heterogeneity of the system studied.[40] Finally, the degree of crystallinity, X_{cr}, a fraction of immobilized polymer referring to the whole polymer fraction, $X_{im,polymer}$, and the amorphous (uncrystallized) polymer fraction, $X_{im,amorph}$, were calculated following eqs. (1)–(5).

The crystallinity degree is large for neat polymers, slightly larger for PEG-4 than PEG-35, and decreases with increasing filler content [Figure 3(b)]. The χ_{cr} values decrease on the second scan (PEG-35) and on quenching for both polymers by ~ 10%. The crystallization [Figure 3(a)], melting [Figure 3(c)] and glass transition [Figure 3(d)] temperatures (Figure 2) are lower for PEG-4 than PEG-35, for both the neat polymers and composites, because of a higher mobility of smaller polymer molecules and a higher amount of the chain ends. The PEG molecules can penetrate into mesopores and macropores of AC particles or voids between adjacent oxide nanoparticles in their aggregates[15,16] during preparation and heating of the composites. The concentration dependences of all the thermodynamic characteristics of the composites are nonlinear functions (Figure 3). This result can be explained by changes in the relative amounts of polymers being in contact with filler

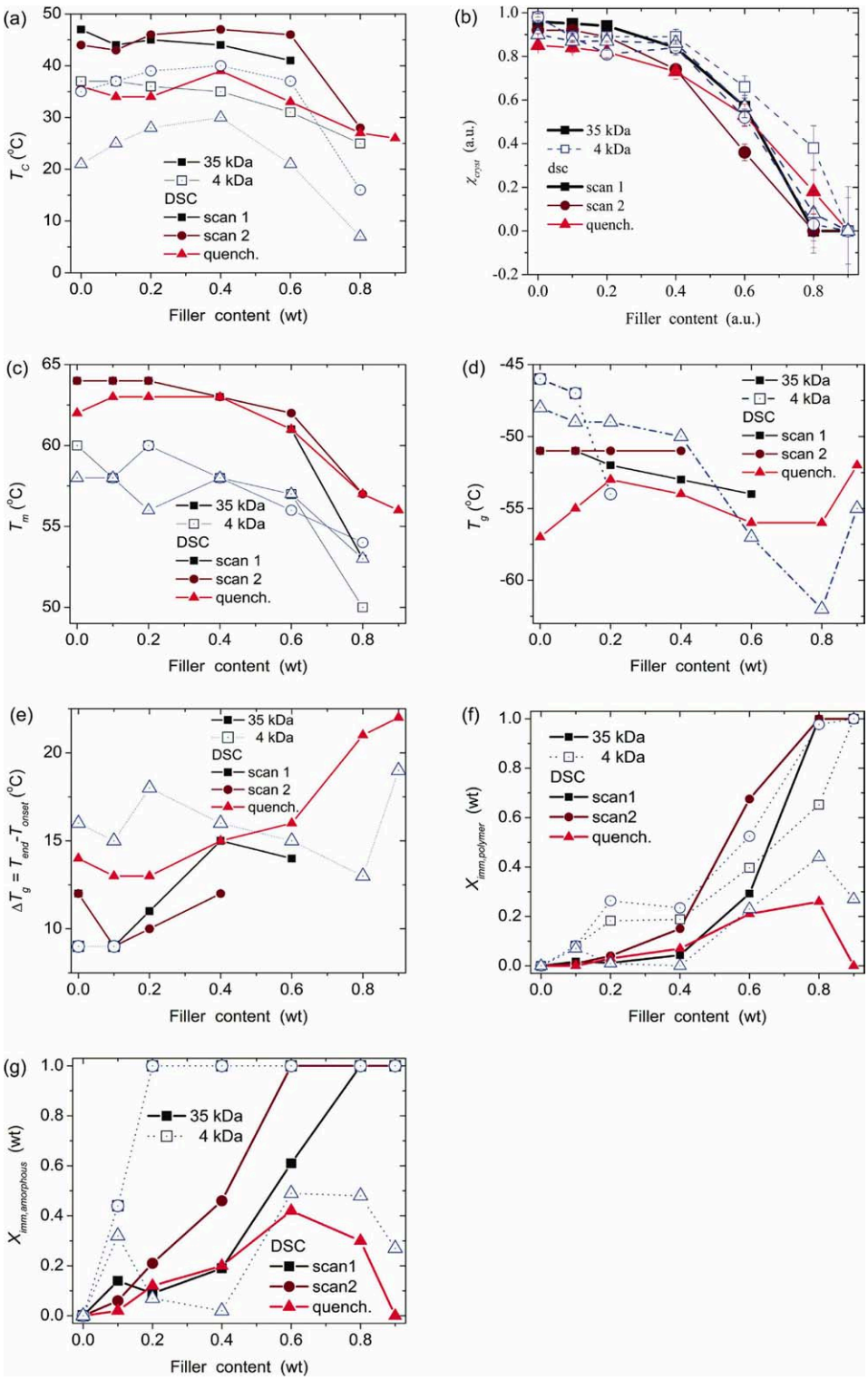

Figure 3. Comparative DSC results for PEG-35/C/ACT (solid symbols) and PEG-4/C/ACT (open symbols) nanocomposites for various thermal treatments: (a) crystallization temperature, (b) degree of crystallinity, (c) melting temperature, (d) glass transition temperature, (e) glass transition temperature interval, (f) fraction of immobilized polymer, and (g) fraction of amorphous immobilized polymer. The lines are guides for the eyes. [Color figure can be viewed in the online issue, which is available at wileyonlinelibrary.com.]

Applied Polymer SCIENCE

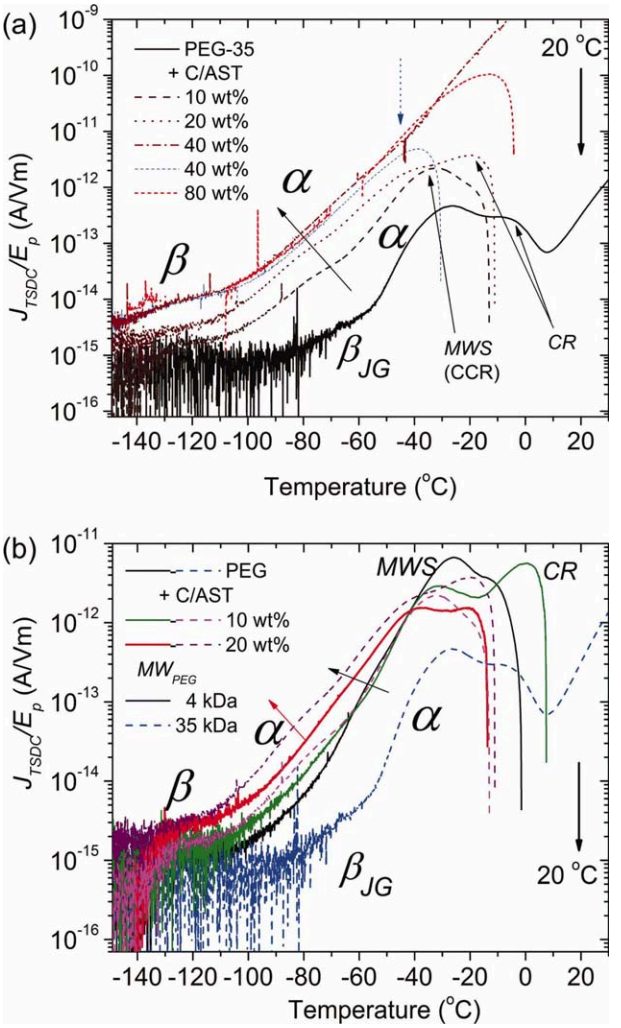

Figure 4. TSDC thermograms for (a) PEG-35 pure and in composites with C/AST, and (b) comparison of the thermograms for PEG-35 and PEG-4 pure and in composites at $C_{C/AST} = 10$ and 20 wt %. [Color figure can be viewed in the online issue, which is available at wileyonlinelibrary.com.]

particles and the corresponding changes in the mobility and chain density in the interfacial layer in comparison with the bulk and neat polymer.

The degree of crystallinity decreases in the nanocomposites [Figure 3(b)], indicating that nanoparticles do not act as crystallization nuclei; in addition, they provide constraints for the diffusion of the polymer chains and growth of crystals.[44] The reduction of the X_{cr} values is particularly pronounced for nanocomposites at $C_{PEG} \leq 40$ wt %, i.e., for PEG adsorbed on solid particles, reflecting constraints to crystallization of polymer chains confined in narrower pores or located at a solid surface, when compared with bulk polymer. As expected, crystallization [Figure 3(a)] and melting temperatures [Figure 3(c)] are, for the neat polymers, smaller for the lower molecular weight polymer.[45] It is interesting that this relationship remains valid for nanocomposites independently of composition. Similar to the degree of crystallinity, the melting temperature decreases with increasing C/AST content in the nanocomposites [Figure 3(c)], indicating smaller and/or less perfect crystals formed at high filler contents.[45] Changes in the crystallization temperature are less pronounced, with exception of the reduction at the highest filler content (80 wt %) for both polymers [Figure 3(a)]. For PEG-4 quenched, first, an increase and then a decrease in the crystallization temperature is observed with increasing filler content. The increase suggests that in this case nanoparticles act as crystallization nuclei.

The glass transition temperature tends to a decrease with decreasing amount of polymer in the composites, and the decrease is more pronounced for PEG-4 [Figure 3(d)]. Notice that here T_g refers to a fraction of amorphous polymer which is not immobilized. The reduction of the T_g value of this amorphous mobile phase can be understood in terms of loosened molecular packing of the chains in voids between nanoparticles in loose aggregates.[46] At the same time, the range of the glass transition shows no systematic variations with composition [Figure 3(e)], in consistency with this explanation. DSC measurements with temperature modulation[40,47,48] provide deeper insight into this effect.

The changes described above and affected by the addition of nanoparticles can be affected by porous AC microparticles (despite $C_{AC} = 10$ wt % only with respect to solids content) because PEG-35/A-300 and PEG-35/AST composites demonstrated distinct concentration dependences[34] different from those of PEG/C/AST observed here. This is due to the differences in the porosity (pore size distribution, PSD), specific surface area, and surface structures of AC and nanooxides.[33–39] The confined space effects are stronger for PEG interacting with AC (composed of nano/meso/macroporous particles) than

Table I. TSDC Peak Temperatures for PEG-35 and PEG-4 Pure and in Composites with C/AST

Samples	X_{poly}	X_{filler}	T_β (°C)	$T_{\beta,JG}$ (°C)	T_α (°C)	T_{MWS} (°C)	T_{CR} (°C)
PEG-35	1	0	−121	−66	−40	−27	−7
PEG90/C/AST10	0.9	0.1	−123	-	−69	−32	-
PEG80/C/AST20	0.8	0.2	−120	-	−73	−35	−19
PEG60/C/AST40	0.6	0.4	−122	-	−60	-	-
PEG20/C/AST80	0.2	0.8	-	-	-	-	−14
PEG-4	1	0	−128	-	−52	−26	−13
PEG90/C/AST10	0.9	0.1	-	-	−53	−31	1
PEG80/C/AST20	0.8	0.2	−118	-	−61	−37	−21

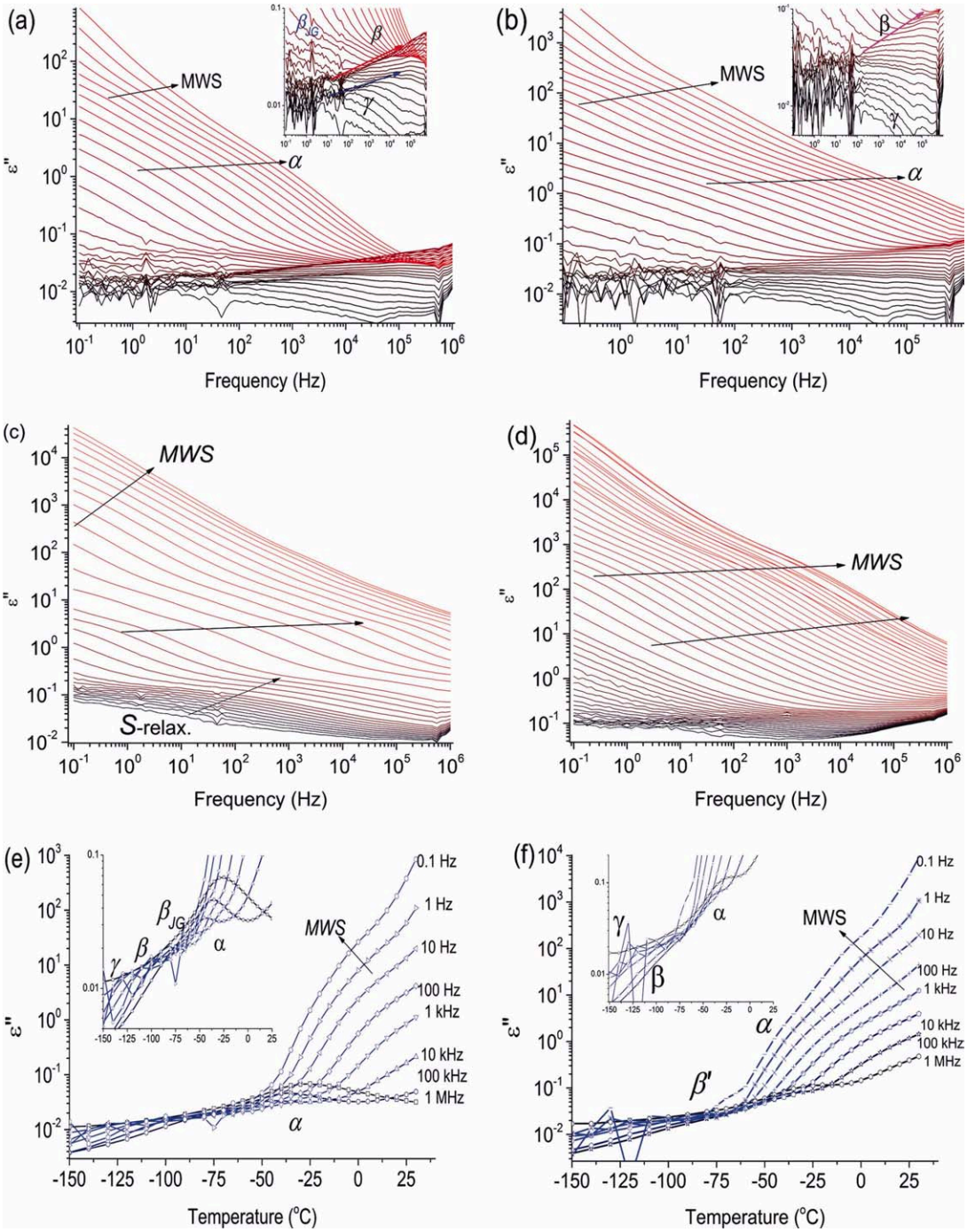

Figure 5. Dielectric loss against frequency, ε'' (f), (a–d) at different temperatures between −150 and 30°C and (e, f) against temperature at different frequencies indicated on the plot for the pure components: (a, e) PEG-35 and (b, f) PEG-4, (c) AST, and (d) C/AST. [Color figure can be viewed in the online issue, which is available at wileyonlinelibrary.com.]

nanooxides (nonporous nanoparticles). However, the interaction energy of PEG with a nanooxide surface (hydrogen bonding and three types of van-der-Waals forces ~ 45 kJ/mol[15]) can be higher than that with AC surfaces (with aromatic structures of carbon sheets and low amounts of O-functionalities ~ 20–30 kJ/mol). Higher mobility of PEG-4 molecules results in a larger fraction of immobilized amorphous polymer than that for PEG-35 [Figure 3(g)]. The PEG monolayer coverage corresponds to C_{pol} = 15–20 wt % for nanooxides.[15,33] Therefore, a fraction of immobilized macromolecules is close to 100% at $C_{pol} \leq 20$ wt % [Figure 3(f)]. Again, a large scattering is observed for the quenched samples (Figure 3). The DSC results show that the nonuniformity (appearing in the mentioned dependences) of the PEG/C/AST composites is a nonlinear function of the C_{pol}

Applied Polymer SCIENCE

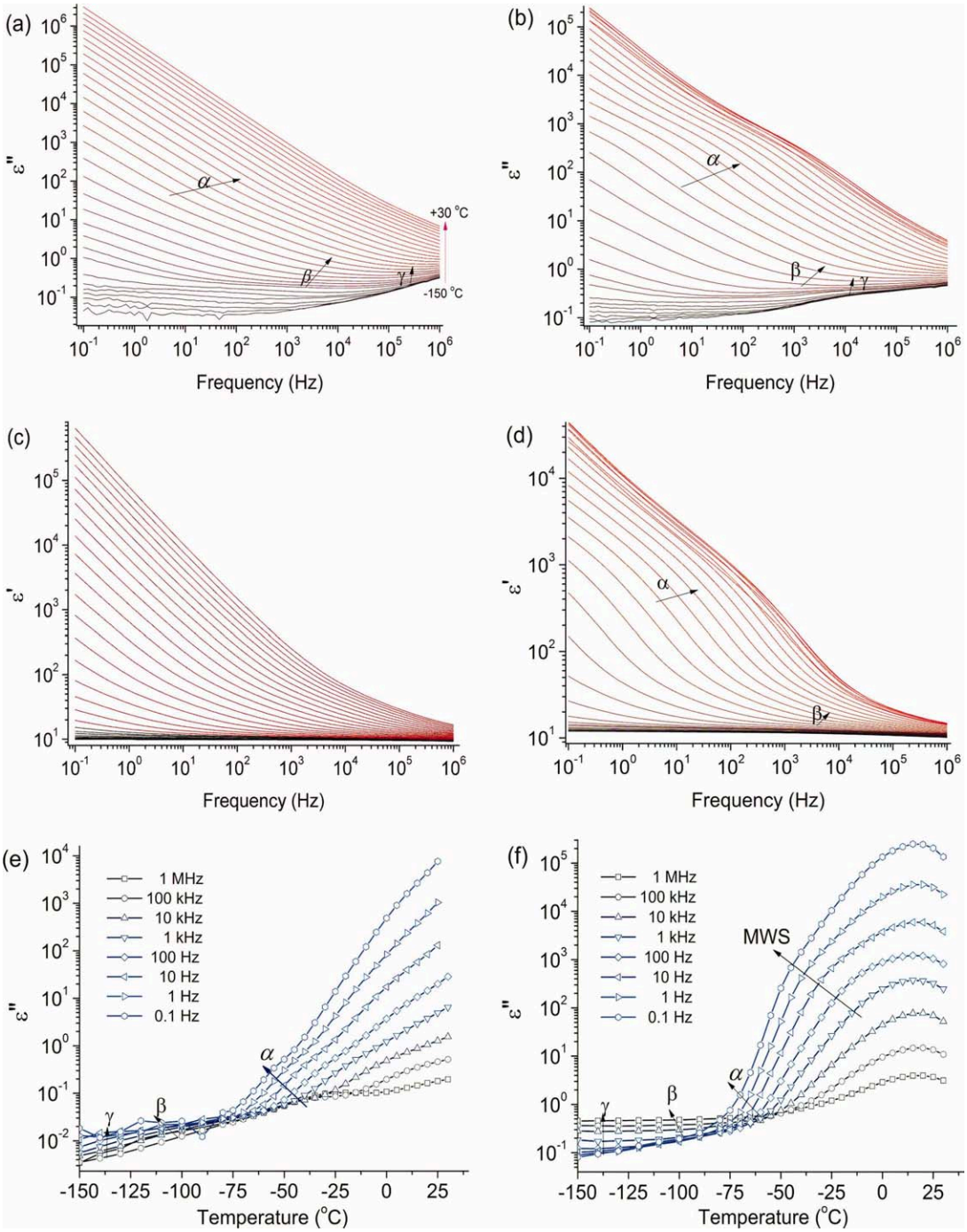

Figure 6. Isothermal (a–d) and isochronal (e, f) DRS measurements of (a, b, e, f) dielectric loss ε'' and (c, d) real part of dielectric permittivity ε' for C/AST/PEG-35 at PEG content of (b, d, f) 10, (a, c) 60 and (e) 90 wt %. [Color figure can be viewed in the online issue, which is available at wileyonlinelibrary.com.]

value. The mentioned structural and energetic features of the composites should affect the relaxation phenomena observed by the TSDC and DRS methods.

TSDC Measurements

TSDC thermograms for all the materials based on PEG-35 are shown in Figure 4(a), whereas Figure 4(b) shows comparative thermograms for PEG-35 and PEG-4 and selected nanocomposites based upon them. Several dipolar relaxations are observed as clear peaks or shoulders. In the order of increasing temperature, these are the local secondary β-relaxation, the Johari-Goldstein process (β_{JG}), and the α-relaxation associated with the glass transition (dynamic glass transition). At temperatures higher than T_g, two additional relaxations are observed associated with conductivity, namely the interfacial MWS relaxation, also known as conductivity current relaxation, and the conductivity relaxation (CR). The first is attributed to accumulation of charges at the amorphous/crystalline polymer and/or polymer/

filler interfaces during polarization and their subsequent release during depolarization.[49] The CR can be better defined in terms of ac measurements as the change from frequency-independent conductivity at low frequencies to frequency-dependent at higher frequencies.[49] Figure 4 shows that the overall TSDC response increases with increasing filler content, reflecting higher electrical conductivity in the nanocomposites. Notice that AC is a conductor but AST is a dielectric because content of semiconductor TiO_2 (bandgap $\sim$ 3.2 eV) is only 1 wt %, but silica and alumina are dielectrics with broad bandgaps. A decrease in the α-relaxation peak temperature with decreasing C_{pol} value is observed in the TSDC thermograms (Figure 4 and Table I) in agreement with the DSC results reported in Figure 3(d). The α-relaxation peak temperature is a good measure for the calorimetric T_g, mainly because of the similar time scale of the two techniques.[40,42] Changes in the β-relaxation temperature with composition are smaller, especially for PEG-35 (Table I), because the α-relaxation reflects segmental dynamics with a characteristic length scale of a few nm (cooperativity length of the glass transition), whereas the sub-T_g β-relaxation is a local one with a characteristic length scale less than 1 nm.[50] Similar to the α-relaxation, the MWS relaxation shifts systematically to lower temperatures with increasing filler content, following the shift of T_g to lower temperatures. This shift is less systematic for the CR relaxation (Table I). A certain scattering or deviations in the characteristic dependences measured by TSDC, as well as by DSC, can be explained by nonuniform distribution of filler particles ($C_{pol} > 50\%$) or polymer molecules ($C_{pol} < 50\%$) in the composites (Figure 1), as well as changes in the fractions of molecules adsorbed in broad pores of AC microparticles or contacting nonporous oxide nanoparticles.

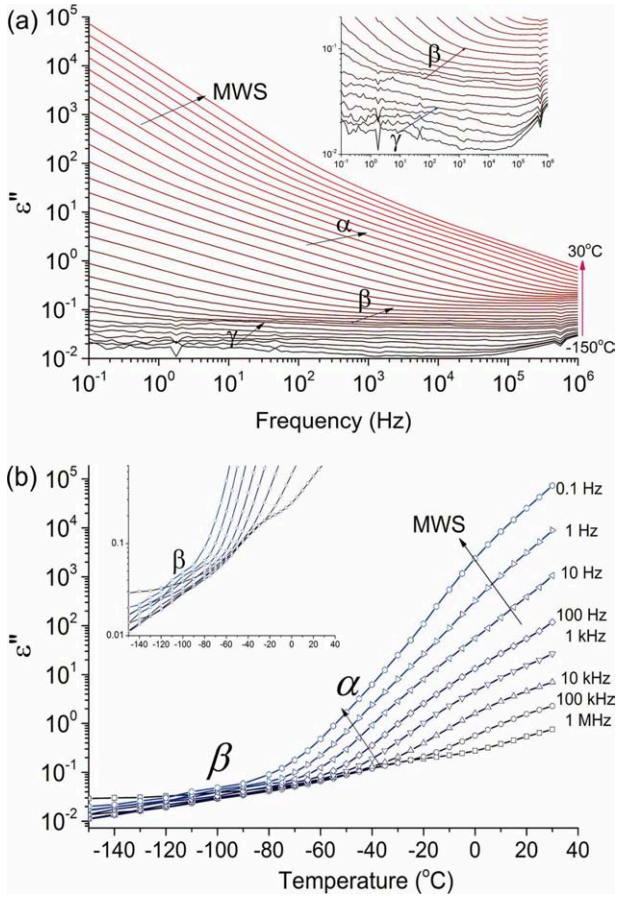

Figure 7. DRS data (a) $\varepsilon''(f)$ and (b)$\varepsilon''(T)$ for PEG-4/C/AST nanocomposites at C_{PEG} = 80 wt %. [Color figure can be viewed in the online issue, which is available at wileyonlinelibrary.com.]

DRS Measurements

Figures 5–8 show raw DRS data, real part of dielectric permittivity, ε', imaginary part of dielectric permittivity (dielectric loss), ε'', and a loss factor, tan $\delta = \varepsilon''/\varepsilon'$, for selected materials, which are representative for all the materials studied. The data are shown in the form of isothermal $\varepsilon'(f)$ and $\varepsilon''(f)$ plots, where f is the frequency of the applied field with temperature of measurements as a parameter, typically varied from −150 to 30°C in steps of 5 or 10°C (depending on the process studied). Alternatively, isochronal (constant frequency) plots are shown, $\varepsilon''(T)$, e.g., in Figure 5(e), with the frequency as a parameter. For these isochronal plots, where the relaxations may be observed more clearly and comparison with TSDC thermograms is more straightforward, the data have been recorded isothermally and replotted. Finally, 3D plots of tan $\delta = \varepsilon''/\varepsilon'$ as a function of both frequency and temperature, richer in information, are shown in Figure 8 for the neat polymers and two PEG-35 nanocomposites. Data in Figure 5 refer to the pure components, PEG-35, PEG-4, AST, and C/AST, and in Figures 6 and 7 to selected nanocomposites. The insets in selected Figures show details of the measurements. Similar to DSC and TSDC, DRS measurements have been performed at ambient conditions but different temperatures. As a result of the hydrophilicity of the components, the samples contain some humidity adsorbed from air, which may affect the observed relaxations (vide infra).

Several relaxations can be followed in Figures 5–8: the secondary γ and β relaxations, the Johari-Goldstein process (β_{JG}), the segmental (primary) α-relaxation associated with the glass transition, the S-relaxation of hydroxyls on the AST particle surface, and the interfacial MWS relaxation. All these relaxations are thermally activated, shifting to higher frequency with increasing temperature in the isothermal plots or to higher temperature with increasing frequency in the isochronal plots. The frequency dependence of the DRS relaxations is determined by the motion rates of the structural elements giving rise to these relaxations, i.e., bound charges (polar bonds, dipoles) and free charges (protons, ions, or electrons, since AC is a conductor and titania is a semiconductor). Therefore, the relaxation frequency increases with T or vice versa. However, the DRS frequency dependences at different temperatures differ for pure PEG, AST, and C/AST (Figure 5). For AST and C/AST (with adsorbed water), the displacement of the frequency curves with temperature occurs without intersections [Figure 5(c,d)] in contrast to PEG [Figure 5(a,b)], especially for longer molecules of PEG-35. This difference is due to the structural hierarchy of the PEG relaxations depending on both T and f. In the case of AST or C/AST with adsorbed water, the structural hierarchy of the DRS relaxations is absent or much weaker because the mobility of all the particles (H_2O, H^+, H_3O^+, electrons, surface OH, and other

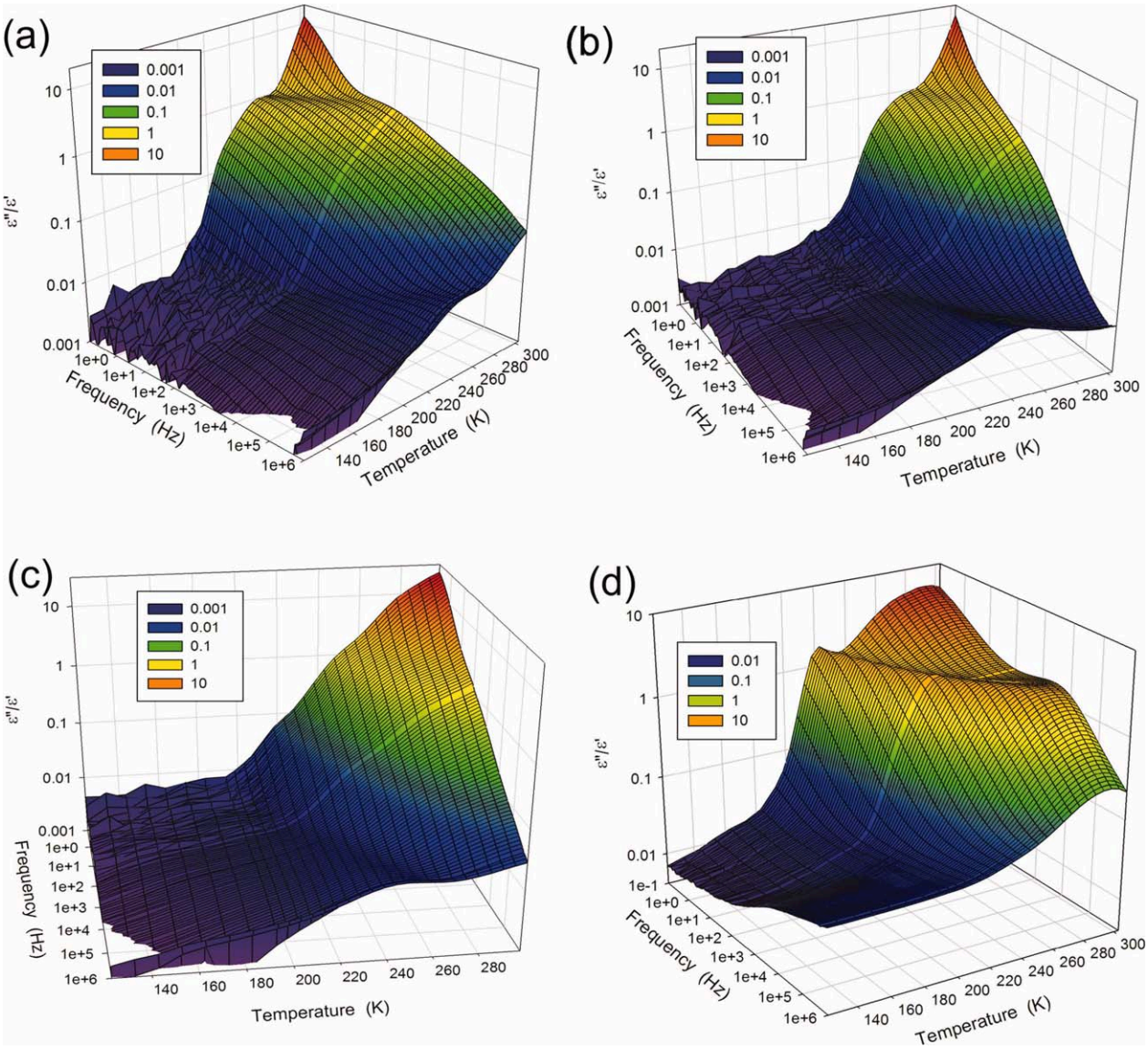

Figure 8. Filler effects on tan $\delta = \varepsilon''/\varepsilon'$ for (a) PEG-4, (b) PEG-35, (c) PEG-35 (90 wt %)–C/AST (10 wt %), and (d) PEG-35 (10 wt %)–C/AST (90 wt %). [Color figure can be viewed in the online issue, which is available at wileyonlinelibrary.com.]

groups) strongly differs from that of polar polymers characterized by the ε'' and ε' values lower by one-two orders of magnitude (Figure 5).

In the case of C/AST/PEG composites, the ε'' and ε' values become larger and changes in their frequency dependences with temperature become smoother at $f > 10^3$ Hz (Figures 6 and 7). Thus, C/AST/PEG with adsorbed water is more polar and with higher mobility of both bound charges (dipoles) and free charges (protons) and water plays the main role in these effects (vide infra). The high ε' and ε'' values at high temperatures and low frequencies for all the materials studied, arising from conductivity,[43] may mask the much weaker dipolar relaxations, which are the main point of interest. In that case, the isochronal plots may become more conclusive comparing examples in Figure 5(a,e).

A decrease in the PEG amount leads to an increase in the dielectric loss (Figure 6) because C/AST with adsorbed water is characterized by much larger ε'' values, when compared with neat PEG (Figure 5). PEG-4 as more mobile than PEG-35 is characterized by greater ε'' values for polymers alone and in composites because of higher concentration of free chain ends (Figures 5–7). A decrease in the polymer content in the composites results in more clear α-relaxation (Figures 6 and 8). However, low temperature relaxations (secondary local motions) are less sensitive to the polymer content. The ε'' values in the range of γ and S relaxations are very low [Figure 5(a,c)].

Comparative DRS data of $\varepsilon''(f)$ on the materials investigated, neat components and the nanocomposites, are shown in Figure 9, in the form of isothermal plots at two different temperatures and of isochronal plots at three different frequencies. In the isothermal plots at −120°C, the response is dominated by the presence of the γ-relaxation in the frequency range 10^2–10^3 Hz in the PEG-rich compositions and of the S-relaxation in the

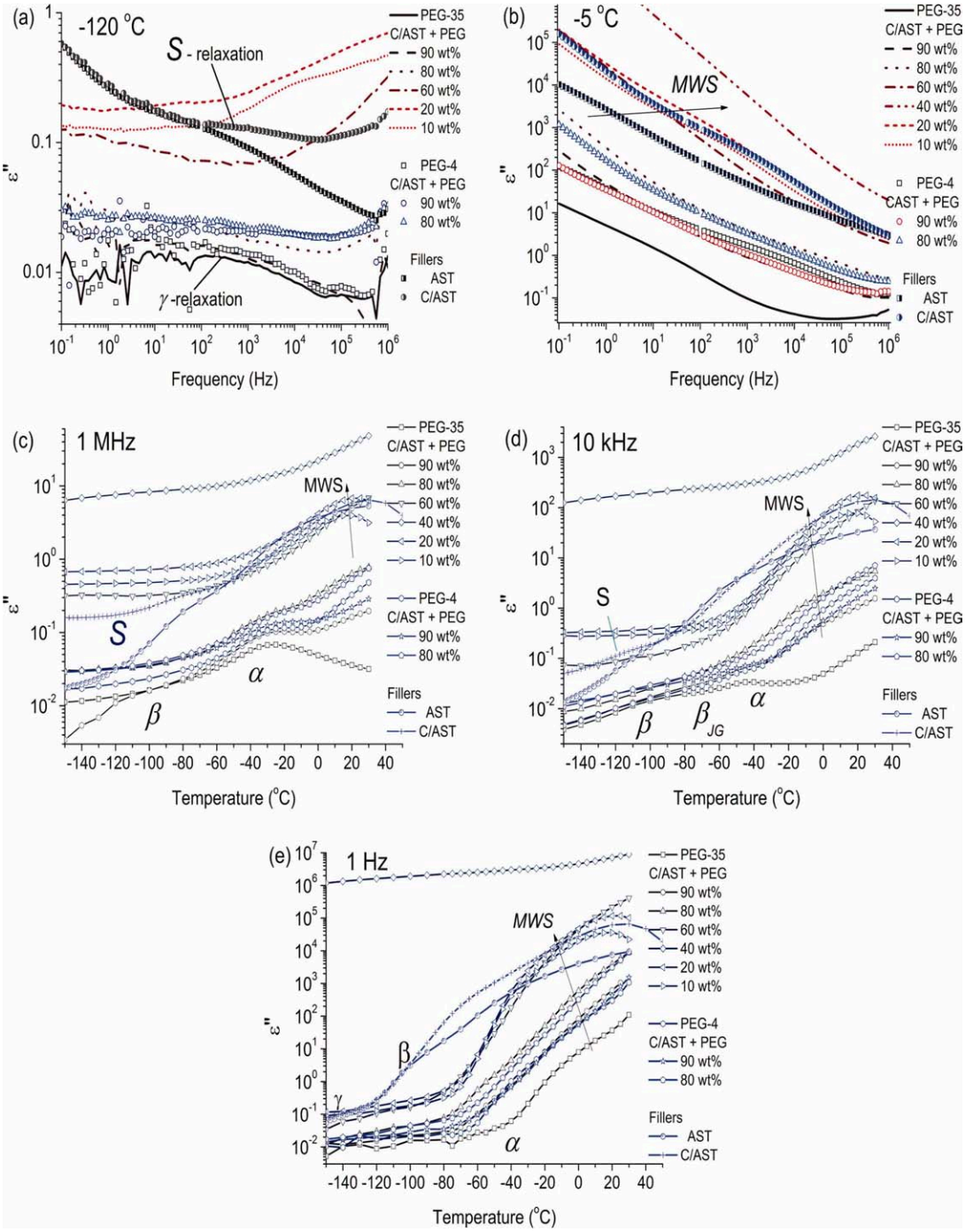

Figure 9. Isothermal (a, b) and isochronal (c–e) comparative DRS data of $\varepsilon''(f)$ on the materials indicated on the plots. [Color figure can be viewed in the online issue, which is available at wileyonlinelibrary.com.]

frequency range 10^3–10^4 Hz in the fillers and the filler-rich compositions. At higher temperature of −5°C, the response is dominated by the interfacial MWS relaxation and conductivity and weaker dipolar relaxations cannot be followed. Similar to the other isochronal plots shown in Figures 5–7, the conductivity effects are suppressed with increasing frequency of presentation, and all the relaxations present in the materials can be followed. The overall response increases on addition of filler to the polymers. It is striking in Figure 9 the behavior of the composite at $C_{\text{PEG-35}} = 40$ wt %, which exhibits maximal ε'' values (even larger than that for AST and C/AST) over the total temperature and frequency ranges. This is probably due to maximum uniformity of this composite, which includes larger amounts of water giving rise to the high response (vide infra).

Figure 10 shows the activation diagram (Arrhenius plot) of the various relaxations followed in the materials under investigation,

Applied Polymer SCIENCE

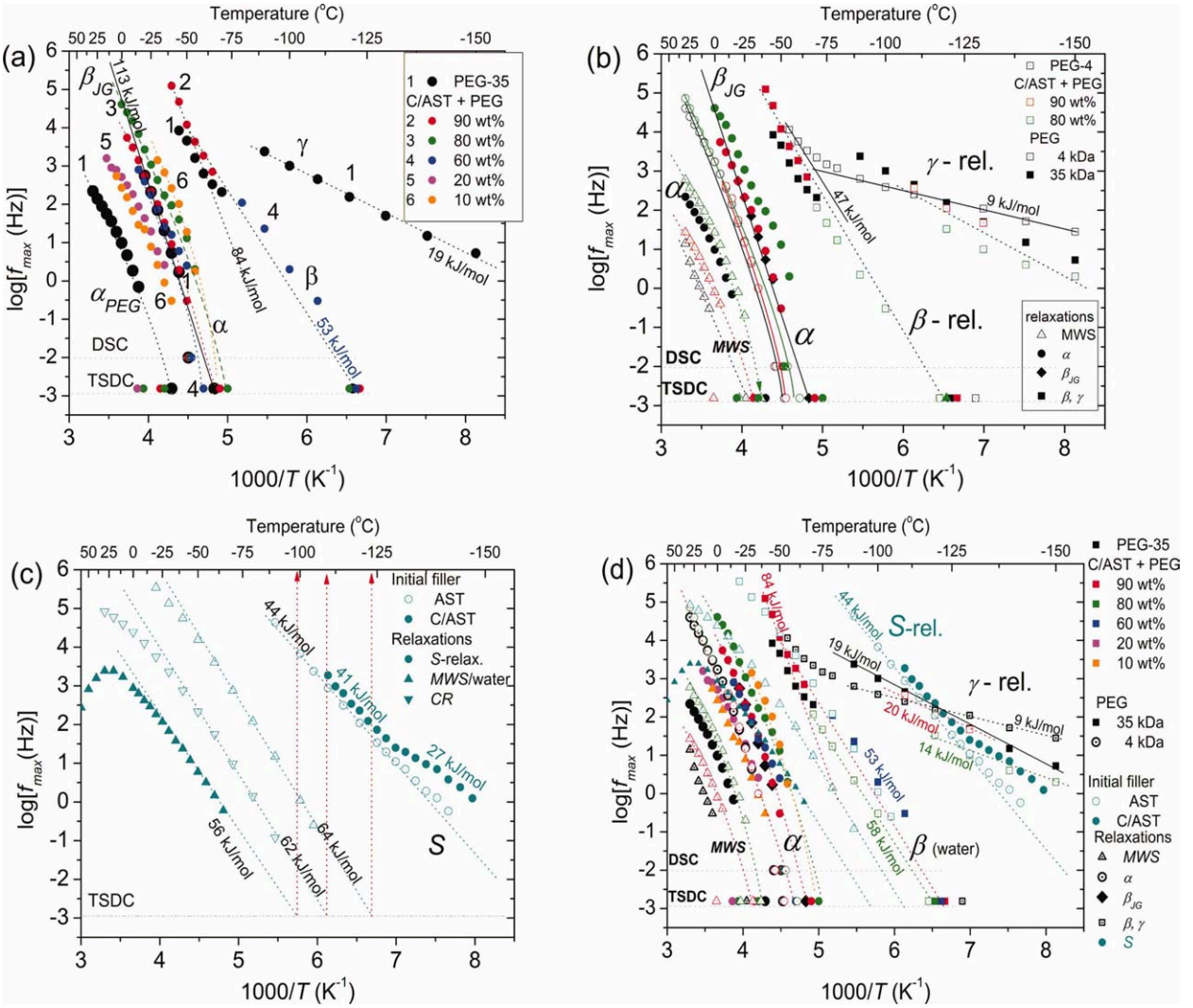

Figure 10. Activation diagram of the various relaxations followed on the materials indicated on the plot. TSDC and DSC data have also been included at the corresponding equivalent frequencies. (a) PEG-35, (b) PEG-4, (c) initial fillers, and (d) overall (only ambient hydration measurements). [Color figure can be viewed in the online issue, which is available at wileyonlinelibrary.com.]

obtained by plotting the logarithm of the corresponding loss peak frequency against reciprocal temperature. Included in the plots are also TSDC data at the equivalent frequency of 1.6 mHz, corresponding to a relaxation time of 100 s at the TSDC peak temperature,[42] as well as DSC data at the equivalent frequency of 10^{-2} Hz at T_g.[40] In general, they are in good agreement with the DRS data, providing the possibility to extend the frequency range of measurements down to low frequencies not easily available by DRS. Typically, a relaxation appearing at lower temperatures is characterized by a lower activation energy (Figure 10). Some of the $\log f_{max}(T^{-1})$ functions demonstrate nonlinear, i.e., non-Arrhenius character, especially the α-relaxation for both neat PEG and composites (which is well known to be described by the Vogel-Tammann-Fulcher equation[50]), as well as for AST and C/AST with adsorbed water. Nevertheless, straight lines were drawn in all cases (shown in Figure 10) to approximately determine values of activation energies. The range of the activation energy of various relaxations is from 9 kJ/mol for PEG-4 and 19 kJ/mol for PEG-35 (γ-relaxation) to 113 kJ/mol (α-relaxation of neat PEG-35). This large difference is due to the different relaxation characters and the different sizes of molar units taking part in each relaxation, from polar bonds (γ-relaxation), to mobility of bound water at −70 to 0°C (S and β-relaxation), to local dynamics of PEG related to the α-relaxation and the glass transition (β_{JG} at $T < T_g$), to cooperative segmental dynamics at $T > T_g$ (α-relaxation), and to interfacial MWS relaxation related to conductivity. Typically, decrease in the PEG content and molecular weight leads to decrease in the activation energy of the corresponding relaxation.

A main conclusion from the activation diagram in Figure 10 is that the α-relaxation becomes faster in the nanocomposites, suggesting a shift of T_g to lower temperatures. In that point, three techniques used, DSC, TSDC, and DRS, demonstrate data consistency. As mentioned above in relation to DSC measurements,

Table II. Water Content of Selected Samples at Two Values of Relative Humidity

Sample	$h_{ambient}$ 40 rh% (wt)	h 75 rh% (wt)
PEG-35	0.005	0.024
PEG90/C/AST10	0.002	0.026
PEG-4	0.009	0.020
AST	0.020	0.060
C/AST	0.030	0.079

the reduction of T_g of the nanocomposites can be attributed to loosened molecular packing of the chains, i.e., increase in the free volume because of features of polymer locations in voids between oxide nanoparticles or in broad pores of AC microparticles.[46] In consistency with this interpretation, the effect is more pronounced for PEG-35 of the higher molecular weight.

Water Effects

Selected samples were exposed to water vapor atmosphere in sealed jars, where the relative humidity (water activity), *rh*, was fixed using appropriate saturated salt solutions in distilled water.[51,52] The samples were exposed for 5–6 days to achieve

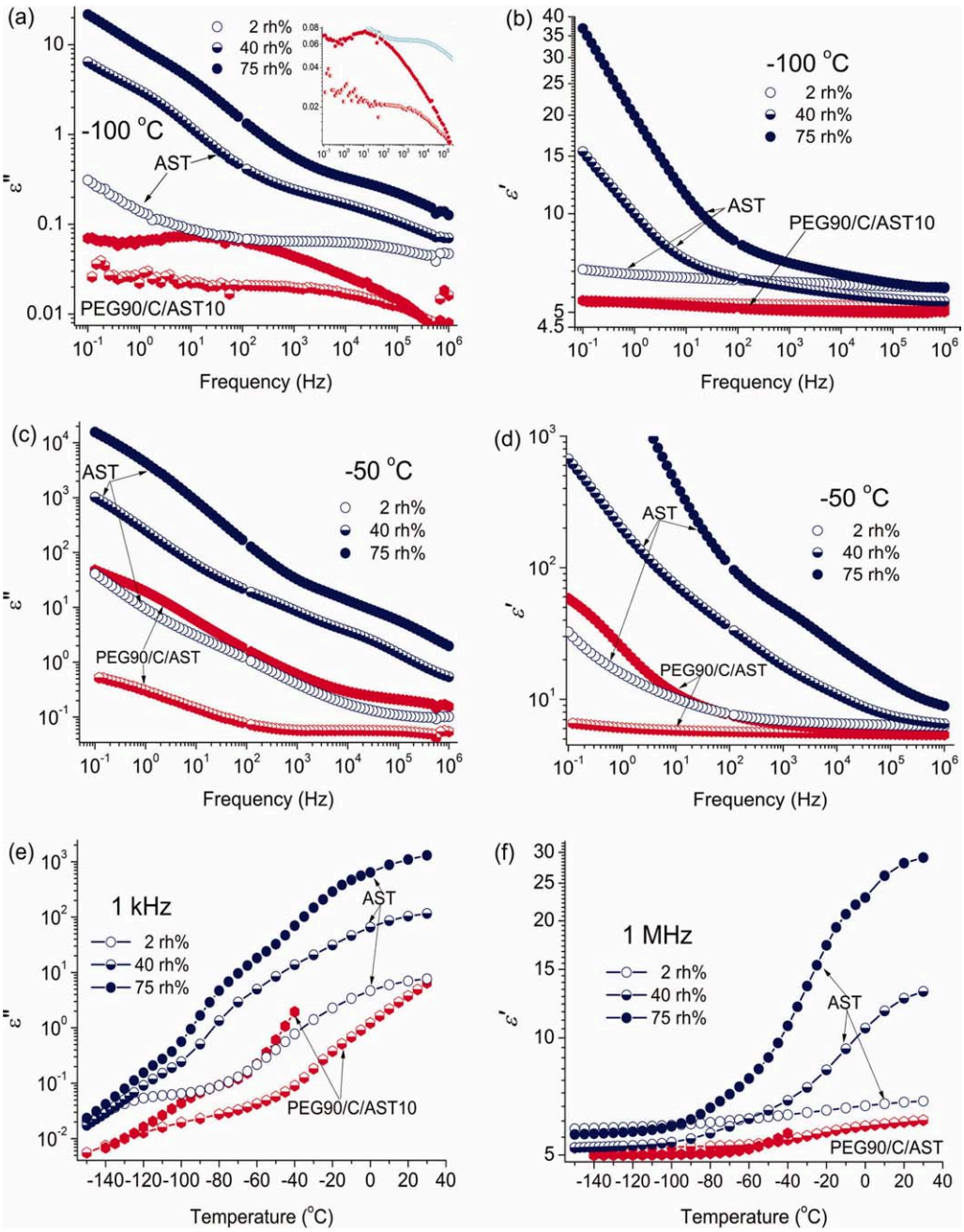

Figure 11. Comparative isothermal (a–d) and isochronal (e, f) DRS spectra of ε' and ε''' for PEG-35(90 wt %)–C/AST (10 wt %) at three levels of relative humidity indicated on the plot. [Color figure can be viewed in the online issue, which is available at wileyonlinelibrary.com.]

equilibrium, which was checked by weighing the samples at distinct time intervals. A Mettler Toledo balance with 10^{-5} g sensitivity was used in these measurements. The weight after equilibrating over P_2O_5 was considered as a dry weight. Once the equilibrium was attained, the hydration (h) was calculated on the dry basis as gram of water per gram of dry material. Table II lists h values for selected materials at two values of relative humidity, and Figure 11 shows representative dielectric data for AST and one nanocomposite, PEG-35 (90 wt %) - C/AST (10 wt %), at three values of relative humidity.

AST is composed of nonporous primary particles. Therefore, despite a large value of the heat of immersion in water (Q = 548 mJ/m^2),[53] it can adsorb only relatively low amounts of water even at rh = 75%. However, this value is larger than that for polymers or composite (Table II). The textural pore volume of AST determined from the nitrogen adsorption at 77.4 K is V_p = 0.25 cm^3/g. The V_p value of AC is much larger (1.26 cm^3/g), but the Q value is lower by order of magnitude (38 mJ/m^2) because of the difference in the specific surface area and the surface structure. However, C/AST adsorbs greater amounts of water than AST. This explains now the larger ε'' and ε' values for C/AST than AST observed in Figure 5. For AST, there is a significant effect of water on the S relaxation [Figure 11(a)]. For both AST and nanocomposite, we observe that water effects become very significant at low frequencies/high temperatures, where conductivity dominates. At low hydration of the composite, the dielectric loss is higher than that of AST at rh = 75%.

CONCLUSIONS

A small addition of AC to AST as a filler of PEG results in significant changes in thermodynamic and relaxation phenomena for PEG/C/AST composites. All their characteristics are nonlinear functions of the polymer (or the filler) content. Maximum nonuniform composite is at $C_{PEG\text{-}35}$ = 40 wt % (corresponding to $\sim$ 61 vol %), which is characterized by maximal values of dielectric permittivity (real part, ε') and dielectric loss, ε'', over the total ranges of frequency and temperature. This can be explained by maximal amounts of adsorbed water in this system. A main conclusion from the DSC results is that the degree of crystallinity decreases in the nanocomposites, in particular at $C_{PEG} \leq$ 40 wt %, i.e., for PEG adsorbed on solid particles. In addition, a significant fraction of the amorphous polymer is immobilized making no contribution to the glass transition. The combined DSC/TSDC/DRS results suggest that the mobile amorphous phase exhibits a lower glass transition temperature and a faster segmental relaxation, when compared with bulk polymer, because of loosened molecular packing of the chains.

ACKNOWLEDGMENTS

This research has been cofinanced by the European Union (European Social Fund—ESF) and Greek national funds through the Operational Program "Education and Lifelong Learning" of the National Strategic Reference Framework (NSRF)—Research Funding Program: Heracleitus II. Investing in knowledge society through the European Social Fund. This work has been financially supported by FP7-PEOPLE-IRSES (COMPOSITUM project No 230790).

REFERENCES

1. Iler, R. K. The Chemistry of Silica; Wiley: Chichester, **1979.**
2. Proceedings of International Conference on Silica Science and Technology "Silica 2001," Sept. 3–6, Mulhouse (France), **2001.**
3. Wingrave, J. A., Ed. Oxide Surfaces; Marcel Dekker: New York, **2001.**
4. Legrand, A. P., Ed. The Surface Properties of Silicas; Wiley: New York, **1998.**
5. Kiselev, A. V.; Lygin, V. I. IR Spectra of Surface Compounds and Adsorbed Substances; Nauka: Moscow, **1972.**
6. Degussa AG. Basic Characteristics of Aerosil, Technical Bulletin Pigments, No 11, Degussa AG: Frankfurt, **1997.**
7. Ray, S. S.; Okamoto, M. *Prog. Polym. Sci.* **2003,** *28*, 1539.
8. Baran, A. A. Disperse Systems Containing Polymers; Naukova Dumka: Kiev, **1986** (in Russian).
9. Lipatov, Yu. S.; Sergeeva, L. M. Adsorption of Polymers; Naukova Dumka: Kiev, **1992** (in Russian).
10. Arshady, R., Ed. Microspheres, Microcapsules and Liposomes, Vol.*2*; Citus Books: London, **1999.**
11. Kiremitci, M.; Pişkin, E. *Int. J. Artif. Organs* **1985,** *8*, 201.
12. Voronin, E. F.; Gun'ko, V. M.; Guzenko, N. V.; Pakhlov, E. M.; Nosach, L. V.; Malysheva, M. L.; Skubiszewska-Zięba, J.; Leboda, R.; Borysenko, M. V.; Chuiko, A. A. *J. Colloid Interface Sci.* **2004,** *279*, 326.
13. Murakami, H.; Kushida, T.; Tashiro, H. *J. Chem. Phys.* **1998,** *108*, 10309.
14. Ngai, K. L.; Riande, E.; Wright, G. B., Eds. Proceedings of the International Discussion Meeting on Relaxations in Complex Systems. J. Non-Cryst. Solids **1994, 172.**
15. Gun'ko, V. M.; Turov, V. V.; Gorbik, P. P. Water at Interfaces; Naukova Dumka: Kiev, **2009** (in Russian).
16. Gun'ko, V. M.; Zarko, V. I.; Goncharuk, E. V.; Andriyko, L. S.; Turov, V. V.; Nychiporuk, Y. M.; Leboda, R.; Skubiszewska-Zięba, J.; Gabchak, A. L.; Osovskii, V. D.; Ptushinskii, Y. G.; Yurchenko, G. R.; Mishchuk, O. A.; Gorbik, P. P.; Pissis, P.; Blitz, J. P. *Adv. Colloid Interface Sci.* **2007,** *131*, 1.
17. Kanaya, T.; Kawaguchi, T.; Kaji, K. *J. Chem. Phys.* **1996,** *105*, 4342.
18. Zorn, R.; Arbe, A.; Colmenero, J.; Frick, B.; Richter, D.; Buchenau, U. *Phys. Rev. E* **1995,** *52*, 781.
19. Colmenero, J.; Arbe, A.; Coddens, G.; Frick, B.; Mijangos, C.; Reinecke, H. *Phys. Rev. Lett.* **1997,** *78*, 1928.
20. Buchenau, U.; Schönfeld, C.; Richter, D.; Kanaya, T.; Kaji, K.; Wehrmann, R. *Phys. Rev. Lett.* **1994,** *73*, 2344.
21. Kanaya, T.; Ishida, T.; Kawaguchi, T.; Kaji, K. *Phys. B* **1995,** *213/214*, 502.
22. Kawaguchi, T.; Kanaya, T.; Kaji, K. *Phys. B* **1995,** *213/214*, 510.
23. Colmenero, J.; Alegria, A.; Alberdi, J. M.; Alvarez, F. *Phys. Rev. B* **1991,** *44*, 7321.
24. Arbe, A.; Alegria, A.; Alvarez, F.; Colmenero, J.; Frick, B. *Prog. Colloid Polym. Sci.* **1993,** *91*, 24.

25. Johari, G. P.; Goldstein, M. *J. Phys. Chem.* **1970,** *74*, 2034.
26. Feng, L.; Zheng, J.; Yang, H.; Guo, Y.; Li, W.; Li, X. *Sol. Energy Mater. Sol. Cells* **2001,** *95*, 644.
27. Bar-Chaput, S.; Carrot, Ch. *J. Appl. Polym. Sci.* **2006,** *100*, 3490.
28. Gajdos, L.; Pietrelli, L.; Ciccarello, A.; Derco, J. *Pol. J. Environ. Stud.* **2007,** *16*, 385.
29. Wang, H.; Yang, Y.; Liang, Y.; Robinson, J. T.; Li, Y.; Jackson, A.; Cui, Y.; Dai, H. *Nano. Lett.* **2011,** *11*, 2644.
30. Gun'ko, V. M.; Zarko, V. I.; Andriyko, L. S.; Leboda, R.; Skubiszewska-Zięba, J.; Janusz, W. *Pol. J. Chem.* **2007,** *81*, 411.
31. Gun'ko, V. M.; Pissis, P.; Spanoudaki, A.; Zarko, V. I.; Nychiporuk, Yu. M.; Andriyko, L. S.; Goncharuk, E. V.; Leboda, R.; Skubiszewska-Zięba, J.; Osovskii, V. D.; Ptushinskii, Yu. G. *J. Colloid Interface Sci.* **2007,** *312*, 201.
32. Sandeman, S. R.; Gun'ko, V. M.; Bakalinska, O. M.; Howell, C. A.; Zheng, Y.; Kartel, M. T.; Phillips, G. J.; Mikhalovsky, S. V. *J. Colloid Interface Sci.* **2011,** *358*, 582.
33. Gun'ko, V. M.; Leboda, R.; Skubiszewska-Zięba, J.; Goncharuk, E. V.; Nychiporuk, Yu. M.; Zarko, V. I.; Blitz, J. P. *Powder Technol.* **2008,** *187*, 146.
34. Klonos, P.; Pissis, P.; Gun'ko, V. M.; Guzenko, N. V.; Pakhlov, E. M.; Zarko, V. I.; Janusz, W.; Skubiszewska-Zięba, J.; Leboda, R. *Colloids Surf. A: Physicochem. Eng. Aspects* **2010,** *360*, 220.
35. Gun'ko, V. M.; Zaulychnyy, Ya. V.; Ilkiv, B. I.; Zarko, V. I.; Nychiporuk, Yu. M.; Ptushinskii, Yu. G.; Pakhlov, E. M.; Leboda, R.; Skubiszewska-Zięba, J. *Appl. Surf. Sci.* **2011,** *258*, 1115.
36. Gun'ko, V. M.; Zarko, V. I.; Turov, V. V.; Oranska, O. I.; Goncharuk, E. V.; Nychiporuk, Yu. M.; Pakhlov, E. M.; Yurchenko, G. R.; Leboda, R.; Skubiszewska-Zięba, J.; Osovskii, V. D.; Ptushinskii, Yu. G.; Derzhypolskyi, A. G.; Melenevsky, D. A.; Blitz, J. P. *Powder Technol.* **2009,** *195*, 245.
37. Gun'ko, V. M.; Kozynchenko, O. P.; Turov, V. V.; Tennison, S. R.; Zarko, V. I.; Nychiporuk, Yu. M.; Kulik, T. V.; Palyanytsya, B. B.; Osovskii, V. D.; Ptushinskii, Yu. G.; Turov, V. A. *Colloids Surf. A: Physicochem. Eng. Aspects* **2008,** *317*, 377.
38. Gun'ko, V. M.; Turov, V. V.; Kozynchenko, O. P.; Nikolaev, V. G.; Tennison, S. R.; Meikle, S. T.; Snezhkova, E. A.; Sidorenko, A. S.; Ehrburger-Dolle, F.; Morfin, I.; Klymchuk, D. O.; Mikhalovsky, S. V. *Adsorption* **2011,** *17*, 453.
39. Gun'ko, V. M.; Meikle, S. T.; Kozynchenko, O. P.; Tennison, S. R.; Ehrburger-Dolle, F.; Morfin, I.; Mikhalovsky, S. V. *J. Phys. Chem. C* **2011,** *115*, 10727.
40. Sorai, M., Ed. Comprehensive Handbook of Calorimetry and Thermal Analysis; Eiley: West Sussex, **2004.**
41. Beaumont, R. H.; Clegg, B.; Gee, G.; Herbert, J. B. M.; Marks, D. J.; Roberts, R. C.; Sims, D. *Polymer* **1966,** *7*, 401.
42. Brauenlich, P., Ed. Thermally stimulated currents in solids, Topics in applied physics, Vol.*37*; Springer: Berlin, **1979.**
43. Kremer, F.; Schönhals, A., Eds. Broadband Dielectric Spectroscopy; Springer-Verlag: Berlin, **2003.**
44. Aranguren, M. *Polymer* **1998,** *39*, 4897.
45. Gedde, U. W. Polymer Physics; Chapman & Hall: London, **1995.**
46. Bershtein, V. A.; Egorova, L. M.; Yakushev, P. N.; Pissis, P.; Sysel, P.; Brozova, L. *J. Polym. Sci. Part B: Polym. Phys.* **2002,** *40*, 954.
47. Xu, H.; Cebe, P. *Macromolecules* **2004,** *37*, 2797.
48. Raftopoulos, K. N.; Janowski, B.; Pielichowski, K.; Pissis, P. *Eur. Polym. J.* **2011,** *47*, 2120.
49. Hedvig, P. Dielectric Spectroscopy of Polymers; Adam Hilger: Bristol, **1977.**
50. Donth, E., Ed. The Glass Transition: Relaxation Dynamics in Liquids and Disordered Materials, Springer series in materials science, Vol *48*; Springer: Berlin, **2001.**
51. Greenspan, L. *J. Res. Natl. Bur. Stand. Sect. A* **1977,** *81A*, 89.
52. Stathopoulos, A.; Klonos, P.; Kyritsis, A.; Pissis, P.; Christodoulides, C.; Rodriguez Hernández, J. C.; Monleón Pradas, M.; Gómez Ribelles, J. L. *Eur. Polym. J.* **2010,** *46*, 101.
53. Gun'ko, V. M.; Yurchenko, G. R.; Turov, V. V.; Goncharuk, E. V.; Zarko, V. I.; Zabuga, A. G.; Matkovsky, A. K.; Leboda, R.; Skubiszewska-Zięba, J.; Janusz, W.; Phillips, G. J. Mikhalovsky, S. V. *J. Colloid Interface Sci.* **2010,** *348*, 546.